INTERFACE

royalsocietypublishing.org/journal/rsif

Research

Cite this article: Kobierski J, Wnętrzak A, Chachaj-Brekiesz A, Filiczkowska A, Petelska AD, Dynarowicz-Latka P. 2021 How the replacement of cholesterol by 25-hydroxycholesterol affects the interactions with sphingolipids: The Langmuir Monolayer Study complemented with theoretical calculations. *J. R. Soc. Interface* **18**: 20210050.
https://doi.org/10.1098/rsif.2021.0050

Received: 8 January 2021
Accepted: 22 February 2021

Subject Category:
Life Sciences–Chemistry interface

Subject Areas:
biophysics

Keywords:
Langmuir monolayers, interactions, sphingolipids, oxysterols

Author for correspondence:
Jan Kobierski
e-mail: jan.kobierski@uj.edu.pl

Electronic supplementary material is available online at https://doi.org/10.6084/m9.figshare.c.5326653.

THE ROYAL SOCIETY PUBLISHING

How the replacement of cholesterol by 25-hydroxycholesterol affects the interactions with sphingolipids: The Langmuir Monolayer Study complemented with theoretical calculations

Jan Kobierski[1], Anita Wnętrzak[2], Anna Chachaj-Brekiesz[2], Anna Filiczkowska[3], Aneta D. Petelska[4] and Patrycja Dynarowicz-Latka[2]

[1]Department of Pharmaceutical Biophysics, Faculty of Pharmacy, Jagiellonian University Medical College, Medyczna 9, 30-688 Kraków, Poland
[2]Faculty of Chemistry, Jagiellonian University, Gronostajowa 2, 30-387 Kraków, Poland
[3]Faculty of Physics, Astronomy and Applied Computer Science, Jagiellonian University, Łojasiewicza 11, 30-348 Kraków, Poland
[4]Faculty of Chemistry, University of Bialystok, Ciołkowskiego 1 K, 15-425 Bialystok, Poland

JK, 0000-0003-3223-0014; AW, 0000-0002-8086-4647; AC-B, 0000-0001-8990-082X; AF, 0000-0001-8411-3798; ADP, 0000-0003-2533-6427; PD-L, 0000-0002-9778-6091

In this paper, a representative of chain-oxidized sterols, 25-hydroxycholesterol (25-OH), has been studied in Langmuir monolayers mixed with the sphingolipids sphingomyelin (SM) and ganglioside (GM_1) to build lipid rafts. A classical Langmuir monolayer approach based on thermodynamic analysis of interactions was complemented with microscopic visualization of films (Brewster angle microscopy), surface-sensitive spectroscopy (polarization modulation–infrared reflection–absorption spectroscopy) and theoretical calculations (density functional theory modelling and molecular dynamics simulations). Strong interactions between 25-OH and both investigated sphingolipids enabled the formation of surface complexes. As known from previous studies, 25-OH in pure monolayers can be anchored to the water surface with a hydroxyl group at either C(3) or C(25). In this study, we investigated how the presence of additional strong interactions with sphingolipids modifies the surface arrangement of 25-OH. Results have shown that, in the 25-OH/GM_1 system, there are no preferences regarding the orientation of the 25-OH molecule in surface complexes and two types of complexes are formed. On the other hand, SM enforces one specific orientation of 25-OH: being anchored with the C(3)–OH group to the water. The strength of interactions between the studied sphingolipids and 25-OH versus cholesterol is similar, which indicates that cholesterol may well be replaced by oxysterol in the lipid raft system. In this way, the composition of lipid rafts can be modified, changing their rheological properties and, as a consequence, influencing their proper functioning.

1. Introduction

Biological membranes contain a plethora of diverse lipids that differ in the type and charge of the polar groups, the structure of the polar part (polycyclic or acyl chains of different levels of unsaturation and the type of main backbone (glycerol versus sphingosine) [1]. The main classes of lipids in eukaryotic cells are phospholipids (glycerophospholipids, sphingolipids) and sterols. They are not evenly distributed within the membrane [2,3], i.e. the internal (cytosolic) leaflet of plasma membranes contains mainly phosphatidylethanolamines (PEs) and phosphatidylserines (PSs). By contrast, the outer (extracellular) leaflet is composed of sphingolipids (such as sphingomyelin, SM), glycolipids and phosphatidylcholines (PCs). Cholesterol

© 2021 The Author(s) Published by the Royal Society. All rights reserved.

(Chol) distribution is still controversial [4], as reviewed in [5]. In various organelles, the proportion of particular lipids differs; for example, endoplasmatic reticulum or mitochondria have a low Chol content, in contrast to myelin [6], while mitochondria are practically devoid of SM [7].

Lipids interact with each other in biomembranes. Chol interplays with low-melting-point lipids and high-melting-point lipids [8], which—given the extracellular leaflet—corresponds to PC and SM, respectively. Since natural SMs contain mostly saturated chains as opposed to PCs, such a system can be approximated to a mixture of Chol, saturated (ordered) lipids and unsaturated (disordered) lipids, the behaviours of which have been thoroughly characterized [9]. Stronger interactions and entropically more favourable packing in bilayers were observed for Chol mixed with lipids possessing saturated versus unsaturated chains [10]. These findings have also been found in monolayers: the excess free enthalpy changes determined for mixtures of Chol with saturated compared with unsaturated phospholipids [11,12] proved the existence of stronger interactions in the former system. Not only are the interactions of the hydrophobic parts important, but also the nature of the polar group. Namely, Chol has been found to have an affinity for strongly hydrated, bulky polar groups, such as those in SM [13] or gangliosides [14], resulting from the presence of a sphingoid base that is capable of forming hydrogen bonds. Coalescence of Chol and SM results in membrane microdomains, called lipid rafts [15]. These are defined as heterogeneous, relatively stiff and extremely dynamic structures surrounded by plasma membrane phospholipids (mainly PCs). It is interesting that rafts can also bind specific proteins [16]. In the current scientific literature, there are a lot of biochemical studies confirming that lipid rafts are involved in physiological processes, such as signal transduction [17], protein sorting [18] and membrane polarization [19]. Recently, lipid rafts have also been associated with the entry of enveloped viruses (including HIV [20], coronaviruses [21–23] or Zika virus [24,25]) and various types of toxins [26] into cells.

Although the formation of SM–Chol complexes in model studies (e.g. Langmuir monolayers) explains the formation of rafts in membranes, their existence in natural cells is still debatable [27,28] because of problems with their visualization. However, the presence of Chol and SM in the membrane is certainly essential. The simplest model of lipid rafts is the mixture of SM and Chol [29,30], corresponding to the strongest interactions between these lipids (Chol : SM films of 1 : 2 proportion). More complex models of lipid rafts also involve phospholipids (1-palmitoyl-2-oleoyl-sn-glycero-3-phosphocholine (POPC) + Chol + SM) and gangliosides (POPC + Chol + SM + GM_1) [31].

Changes in lipid patterns that occur during pathological processes (such as neurodegenerative diseases or cancer) may lead to the reorganization of lipid rafts. This may result in the destabilization and incorrect functioning of the entire cell [32,33]. Many cell pathological processes are associated with oxidative stress. Consequently, Chol homeostasis concentration of its oxidized forms (so-called oxysterols) is increased [34]. Oxysterols, similarly to Chol, can affect the properties of membranes [35], and the presence of an additional polar group can significantly modify the interactions with other membrane components. Modifications of such interactions have been described in the literature [35,36].

In this study, we have investigated the interactions between a representative of a chain-oxidized oxysterol—25-hydroxycholesterol (25-OH)—and two sphingolipids—GM_1 and SM.

In a recent report [37], we have shown an unusual surface behaviour of 25-OH related to its dual arrangement, i.e. the molecule can be anchored to the water surface with a hydroxyl group at either C(3) or C(25). SM and GM_1 are sphingolipids, which—owing to their chemical structure—form tightly packed structures with Chol. We believe that in pathological processes, while the amount of oxysterols increases, Chol molecules involved in lipid rafts may be replaced with their oxidized form. Therefore, our experiments aim to show how replacing Chol with 25-OH oxysterol modulates the mutual interactions in membrane domains and their physicochemical properties, such as packing or stiffness.

To gain insight into the nature and strength of these interactions, the Langmuir monolayer method was applied. Complemented with Brewster angle microscopy (BAM) and polarization modulation–infrared reflection–absorption spectroscopy (PM-IRRAS), this clarifies the surface behaviour in monolayers mimicking lipid rafts. The analysis was extended to theoretical calculations (dimer formation and molecular dynamics). The proposed approach allows us to characterize the interactions between 25-OH and specific membrane lipids and present their biological implications.

2. Material and methods

2.1. Materials

Natural sphingolipids of high purity (greater than 99%): SM (isolated from chicken egg) and GM1 (isolated from the bovine brain), as well as Chol and 25-OH, were supplied by Avanti Polar Lipids. Spreading solutions of lipids were prepared in chloroform stabilized with ethanol (purchased from Aldrich; HPLC grade, greater than or equal to 99.9%). Appropriate volumes of stock solutions were mixed to obtain aliquots for the Langmuir studies. Deionized ultrapure water from a Millipore system with a resistivity of 18.2 MΩ cm and a surface tension of 72.8 mN m^{-1} at 20°C was used as a subphase.

2.2. Methods

2.2.1. Langmuir monolayer technique and Brewster angle microscopy

The experiments were performed with a Langmuir trough (KSV NIMA KN 2002; total area = 273 cm^2, double barriers) placed on an anti-vibration table. Langmuir monolayers were obtained by spreading an aliquot of the mixed solution with a microsyringe onto the subphase (20 ± 0.5°C). Surface pressure was measured as being accurate to ±0.1 mN m^{-1} using a Wilhelmy plate made of ashless chromatography paper (Whatman Chr1). Each isotherm was repeated at least three times to ensure the experimental curves' reproducibility to ±2 $Å^2$ $molecule^{-1}$. BAM experiments were performed with an UltraBAM instrument (Accurion GmbH, Goettingen, Germany) installed over the KSV 2000 (total area = 700 cm^2, double barriers) Langmuir trough. The microscope was equipped with a 50 mW laser emitting p-polarized light at a wavelength of 658 nm, a 10× magnification objective, a polarizer, an analyser and a CCD camera. BAM images show monolayer fragments of 720 µm × 400 µm.

2.2.2. Polarization modulation–infrared reflection–absorption spectroscopy

PM-IRRAS spectra were obtained using the KSV PM-IRRAS instrument installed over the KSV NIMA KN 1003 (total area = 273 cm^2, double barriers) Langmuir trough. The angle of incidence was set to 80°. A Langmuir monolayer was prepared as described above, compressed to the selected surface pressure

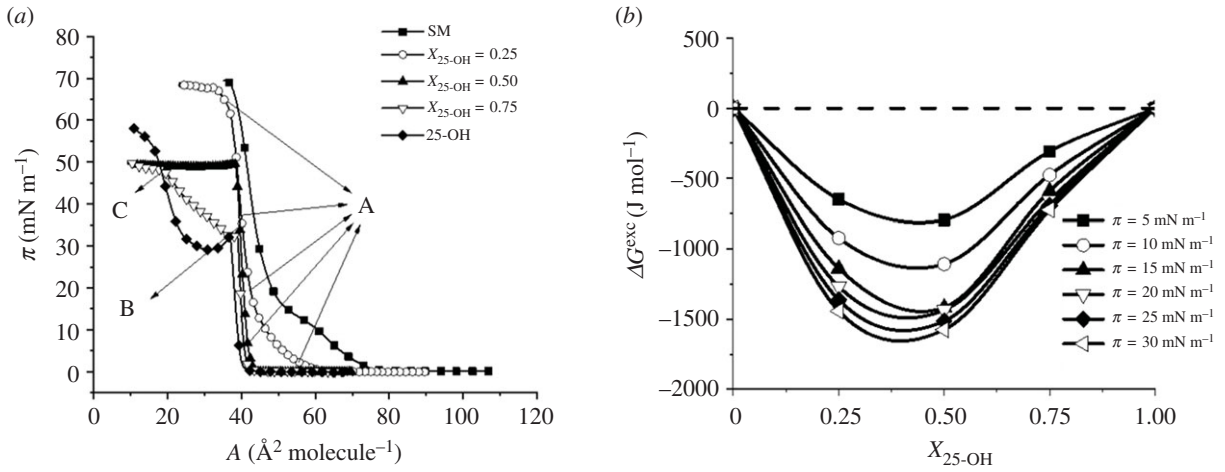

Figure 1. π–A isotherms registered for mixed systems of 25-OH with SM (*a*); changes in free enthalpy of mixing (ΔG^{exc}) as a function of 25-OH content (*b*).

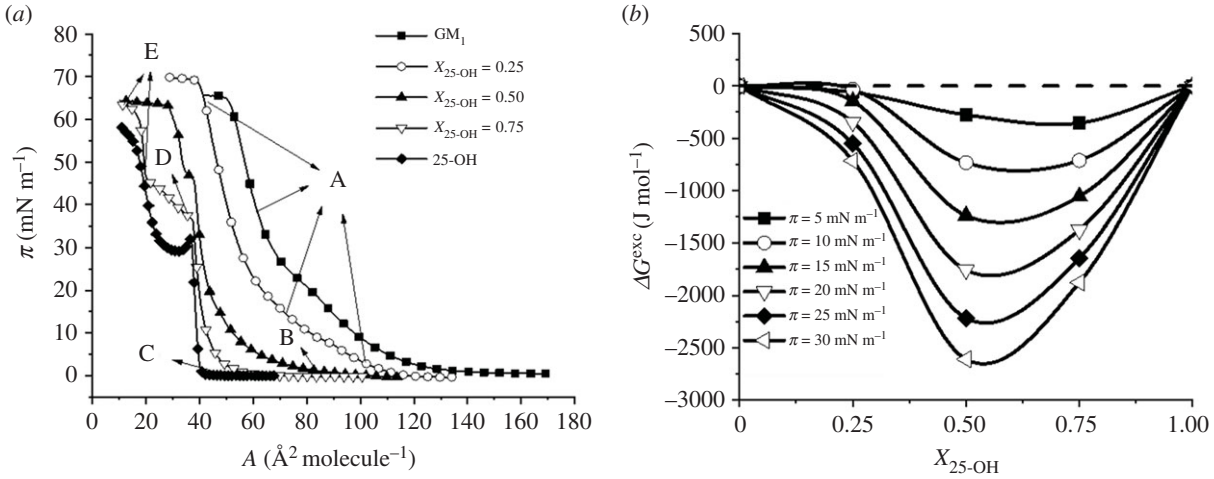

Figure 2. π–A isotherms registered for mixed systems of 25-OH with GM_1 (*a*); changes in free enthalpy of mixing (ΔG^{exc}) as a function of 25-OH content (*b*).

value and stabilized for 5 min. Each spectrum was a result of 6000 scans with a spectral resolution of 8 cm^{-1}. Measurements were performed at least two times to ensure reproducibility of the results. The obtained spectra were processed with OPUS software: background subtraction, baseline correction (straight lines, 1×) and smoothing (Savitzky–Golay method).

2.2.3. Theoretical calculations

The dipole systems' geometry optimization was performed using density functional theory (DFT) modelling employing the Gaussian 16 software package [38]. All calculations were performed using the B3LYP functional [39–42] with a 6–311G(d,p) basis set [43,44] and the D3 version of Grimme's empirical dispersion with the original D3 damping function [45]. Systems were optimized using the default UltraFine integration grid, default integral cut-offs and a combination of EDIIS and CDIIS tight convergence procedures, with no Fermi broadening. The base superposition error was eliminated by using the counterpoise correction.

Molecular dynamics was calculated in the Amber 2018 software [46]. Simulated systems consisted of two monolayers, having 77 molecules of SM and 51 25-OH molecules, and 56 molecules of GM_1 and 56 25-OH molecules, in two mutual orientation of molecules (the polar group of the sphingolipids neighbouring with either the C(3)–OH or C(25)–OH group of 25-OH), separated by 30 000 water molecules. For GM_1, 128 Na ions were added to neutralize the system. A vacuum of 100 Å was left in the Z-direction between adjacent periodic boxes to avoid the monolayers interacting. A general amber force field [47] was used for lipid molecules. A TIP3P model was used to simulate water molecules [48].

The energy of the systems was minimized by 50 000 steps. Systems were equilibrated by 75 000 steps with a 0.001 ps time step, followed by 300 000 steps with a 0.002 ps time step. Production calculations were carried out under an isothermal–isobaric ensemble with constant surface tension (NPγT) with a 0.002 ps time step. The temperature was set at 293 K, and a Langevin thermostat was used. A Berendsen barostat was used to control the pressure at 1 bar. The simulation was carried out for 80 ns, and the last 10 ns were used for analysis.

3. Results and discussion

3.1. Analysis of miscibility and interactions in Langmuir films

In the first step of our studies, the surface pressure–area isotherms for 25-OH/SM and 25-OH/GM_1 monolayers differing in oxysterol content ($X = 0.25$, 0.50 and 0.75) were recorded. The results were used for quantitative analysis of the interactions with the excess free enthalpy of mixing $\Delta G^{exc} = N_A \int (A_{12} - (A_1X_1 + A_2X_2))\mathrm{d}\pi$ [49,50]. The obtained results are presented in figures 1 and 2. Textures of floating layers (visualized with BAM) are shown in figures 3 and 4.

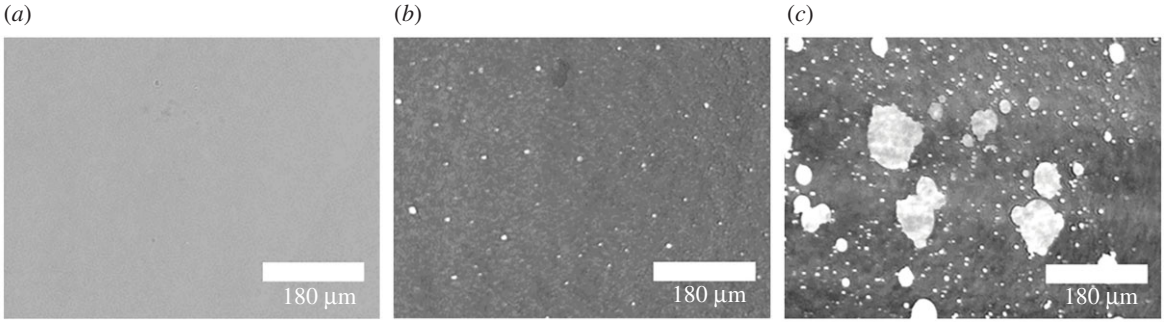

Figure 3. BAM images of mixed films formed by 25-OH and sphingomyelin at surface pressure values designated in the isotherms in figure 1.

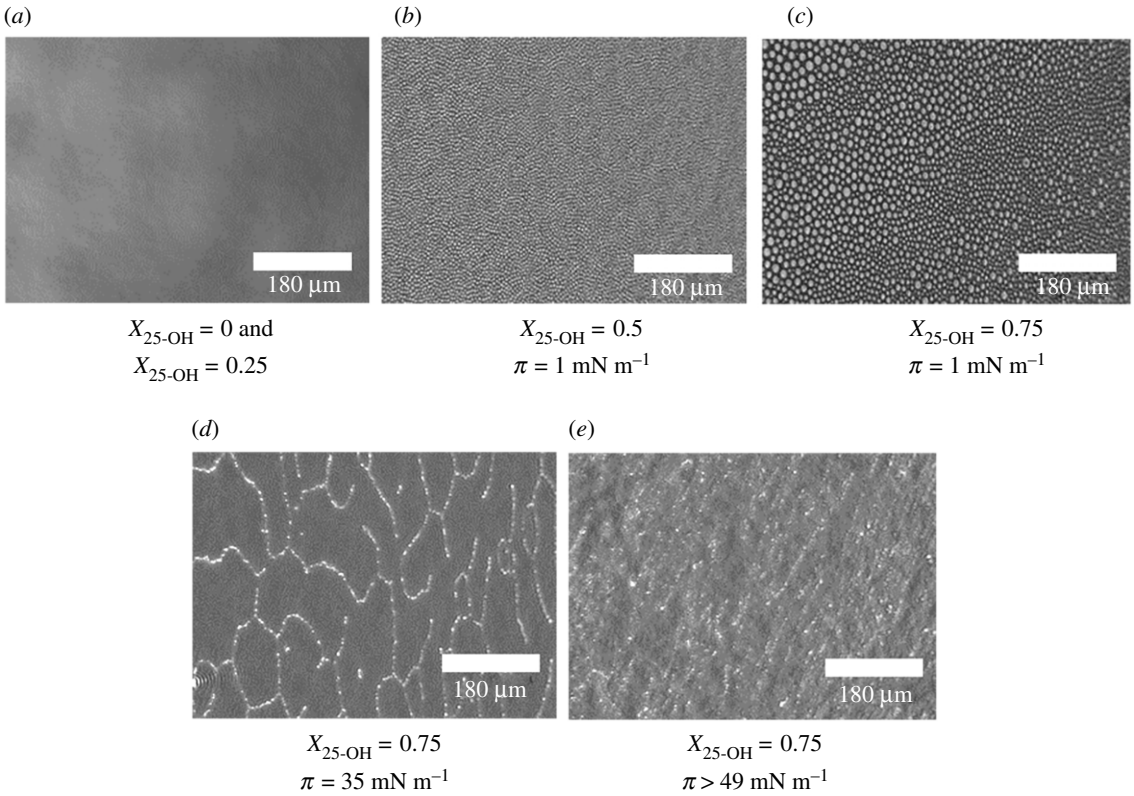

Figure 4. BAM images of mixed films formed by 25-OH and ganglioside GM_1 at surface pressure values designated in the isotherms in figure 2.

Additionally, based on experimental curves, miscibility diagrams were made (electronic supplementary material, figures S1 and S2).

Isotherms registered for mixed systems are situated between those for single-component films. Even a small addition of oxysterol ($X_{25\text{-OH}} = 0.25$) significantly shifts the isotherm towards smaller areas per molecule and causes the inflection associated with the phase transition, observed in the isotherm of pure SM, to disappear. For mixtures of an oxysterol mole fraction of $X_{25\text{-OH}} = 0.25$ and $X_{25\text{-OH}} = 0.50$, one collapse is observed (figure 1*a*), proving the miscibility of the components (confirmed by a homogeneous BAM image (figure 3*a*)). Analysis of the excess free enthalpy of mixing, ΔG^{exc} (figure 1*b*), shows that, for all analysed mixed 25-OH/SM systems, negative deviations from ideal behaviour are observed, indicating that stable surface complexes may be formed. Their stoichiometry was determined based on the minimum in the ΔG^{exc} ($X_{25\text{-OH}}$) curves and is in the range of $X_{0.25} = 0.37$–0.40.

In turn, for $X_{25\text{-OH}} = 0.75$, two collapses are visible: the first at $\pi = 33.5$ mN m^{-1} (slightly higher than that for pure 25-OH), and the second at $\pi = 49.5$ mN m^{-1} (coinciding with the collapse pressure for the mixture of $X_{25\text{-OH}} = 0.50$). Considering this, it can be supposed that there is an excess of unbound oxysterol in this mixture—the first collapse can be attributed to the transition of free (unbound) oxysterol from two dimensions to three. In the miscibility diagrams, the corresponding phases are denoted as P1 and P2 (see electronic supplementary material, figure S1). This can be additionally supported with BAM images (figure 3*b*), where bright domains appear exactly at the first collapse, indicating the 'ejection' of oxysterol molecules from the film. The second collapse results from the collapse of all the mixture components, i.e. 25-OH/SM complexes and bilayers formed by unbound oxysterol (figure 3*c*).

Let us proceed to the analysis of the other investigated system.

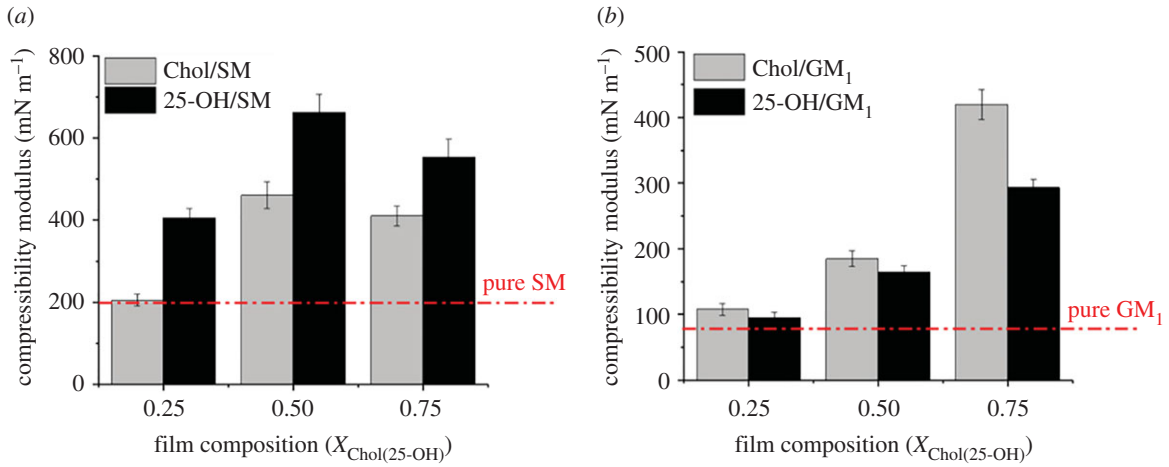

Figure 5. Changes in compressibility modulus values in mixed systems of 25-OH and Chol with SM (*a*) and GM_1 (*b*) at 30 mN m^{-1}. The dashed red line represents the compressibility modulus for pure sphingolipid. Bars indicate the uncertainty obtained by the exact differential method.

In this case, isotherms for mixed films also lie between those for pure components (25-OH and GM_1). The addition of oxysterol shifts the transition visible on the isotherm of pure GM_1 (attributed to the phase transition between the liquid expanded and liquid condensed state [51]) from 20 to 15 mN m^{-1} (for $X_{25\text{-OH}} = 0.25$ and $X_{25\text{-OH}} = 0.50$). Nevertheless, the film topography images of pure GM_1 and its mixtures of $X_{25\text{-OH}} = 0.25$ are completely homogeneous (in the entire range of the studied pressures; an example image is presented in figure 4*a*). However, the behaviour is unclear for mixtures with a higher oxysterol content. Low-pressure BAM images (figure 4*b*,*c*) show the formation of circular domains, which disappear with increasing pressure (at about 15 mN m^{-1}). For these mixtures, more than one inflection is observed in the course of the isotherms. This is especially interesting for an equimolar mixture. Based on ΔG^{exc} analysis, it can be concluded that stable surface complexes of 1 : 1 stoichiometry are formed (figure 2*b*). Therefore, one collapse should be expected to appear in the isotherm. However, two collapses are visible in the course of the isotherm. The situation we are dealing with may result from a different arrangement of 25-OH molecules in the above-mentioned surface complexes with GM_1 (as indicated in the phase diagram, electronic supplementary material, figure S2): when 25-OH is anchored on the water surface with the OH group in the C3 position (↑) or with the OH in the tail (C25) (↓). GM_1 can be anchored to the surface only with its head group. In the case of a film containing a mole fraction of 25-OH = 0.75, we are dealing with a mixture containing an excess of oxysterol. Therefore, the first inflection can be related to the two-dimensional to three-dimensional transition of unbounded 25-OH (figure 4*d*), and the second one to the collapse of surface complexes (figure 4*e*). To sum up, we can see that the type of sphingolipid molecule can force changes in the arrangement of oxysterol molecules in complexes and determine their properties, such as stability. In turn, it may change the lipid pattern in rafts and affect their proper functioning. Comparing the interactions in complexes with those in analogous systems with Chol (see electronic supplementary material, figure S3), one can see that the strength of interactions may also be of great importance. The strength of the interactions (reflected in ΔG^{exc} values) shows that the interactions are only slightly weaker (10% less) in the 25-OH/GM_1 system (approx. –2.7 kJ mol^{-1}) than in the analogous Chol/GM_1 system (approx. –3 kJ mol^{-1}). The situation is quite different for mixed systems with SM. Here, the strength of interactions increases (by about 30%) when Chol is replaced by oxysterol (from –1.1 kJ mol^{-1} [52] to –1.6 kJ mol^{-1} at 30 mN m^{-1} and $X = 0.25$). The stoichiometry of the complexes also changes (from $X_{Chol} = 0.33$ to $X_{25\text{-OH}} = 0.40$). However, to better characterize the organization of molecules in mixed layers, PM-IRRAS experiments and theoretical calculations were performed.

3.2. Rheological properties of Langmuir monolayers

In the next stage, we analysed the influence of 25-OH on lipid raft properties during pathological processes (when the level of oxysterols increases). To achieve this goal, we determined molecular packing in the mixed systems: Chol/sphingolipid and 25-OH/sphingolipid by calculating changes in compressibility moduli. Compressibility modulus curves are presented in electronic supplementary material, figure S4. Additionally, values obtained for the surface pressure of 30 mN m^{-1} (corresponding to conditions in biomembranes [53]) have been compared in figure 5.

As can be seen, the addition of 25-OH or Chol into the SM and GM_1 monolayers influences the organization of films from both sphingolipids; however, the organization is different. In the case of SM, even a small addition of oxysterol ($X_{25\text{-OH}} = 0.25$) changes the physical state of the film from liquid to condensed ($C_s^{-1} > 250$ mN m^{-1}). For mixtures with Chol, the change is clearly visible for an equimolar mixture. However, the film stiffening is stronger for the oxysterol-containing system. The situation is different for mixtures with GM_1, where no significant changes in the film's rheological properties are observed when the molar fraction of 0.25 (both Chol and 25-OH) is added. For a 1 : 1 mixture, the film stiffness increases, but the physical state remains the same (liquid state). Only at the highest concentration of both sterols is a significant increase in molecular packing observed. A slightly stronger condensing effect of Chol is observed for all the analysed molar fractions compared with its oxidized derivative.

The obtained results agree with the analysis of thermodynamic interactions (stronger interactions in Chol/GM_1 and 25-OH/SM systems than in Chol/SM and 25-OH/GM_1 mixed films).

Additionally, to show how the sphingolipid layer's stability is affected by the presence of 25-OH, changes in

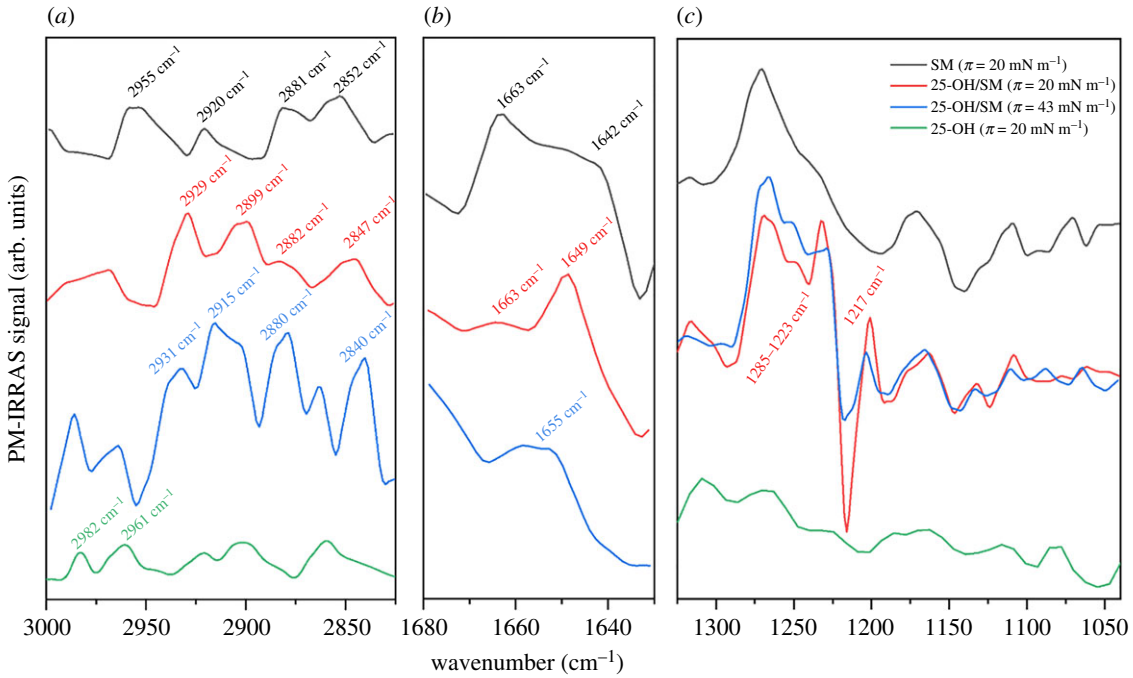

Figure 6. PM-IRRAS spectra of a 25-OH/SM ($X_{25\text{-OH}} = 0.50$) monolayer compared with the spectra of pure components (25-OH and SM) at selected values of surface pressure registered in the spectral regions 3000–2830 (*a*), 1680–1630 (*b*) and 1300–1000 cm^{-1} (*c*).

surface pressure versus time have been recorded and presented in electronic supplementary material, figure S5. For comparison, analogous data for Chol are shown. The obtained dependencies suggest that the studied oxysterol influences the kinetic stability of mixed monolayers at 30 mN m^{-1} to a greater extent than Chol.

3.3. Structural origin of the observed interactions analysed with PM-IRRAS

PM-IRRAS is a complementary tool for the study of Langmuir monolayers, which enables the identification of functional groups involved in interactions with the subphase and between molecules in the monolayer [54,55] and description of the conformation of phospholipid acyl chains [56,57]. Additionally, since the PM-IRRAS signal's intensity is related to the orientation of the moment of transition of individual vibrations, one can estimate the molecular orientation in the layer [58]. In this study, we examined the spectral behaviour of 25-OH/sphingolipid systems compared with the results obtained from pure lipid monolayers (25-OH, SM and GM_1). Let us first discuss the 25-OH/SM ($X_{25\text{-OH}} = 0.50$) mixture (figure 6).

The spectra obtained for the 25-OH/SM system in the C–H stretching region (3000–2800 cm^{-1}) show bands from both components (SM and 25-OH), including characteristic peaks from CH_2 asymmetric stretching in 25-OH (appearing at *ca* 2961 and 2982 cm^{-1}).

It can be noted that the spectrum probed from the mixed film at 20 mN m^{-1} shows some differences in comparison with the pure SM film.

(1) The CH_2 asymmetric stretching band overlaps with its undertone (band at *ca* 2930 cm^{-1}) and with the other band due to the Fermi resonance (band at *ca* 2899 cm^{-1}) [56].
(2) The CH_2 symmetric stretching band is shifted to 2847 cm^{-1}.
(3) CH_3 symmetric and asymmetric stretching bands become less intensive.

These observations (especially the spectral position of the CH_2 stretching bands) suggest that hydrocarbon chains in a mixed monolayer at a surface pressure of 20 mN m^{-1} are probably in a more ordered *all-trans* conformation [57]. When the film is compressed to 43 mN m^{-1}, the intensity of the signal (at 2880 cm^{-1}) from CH_3 symmetric stretching vibrations increases, indicating a decrease in hydrocarbon chain ordering [59] and/or changes in molecular orientation [58]. The bands from the main functional groups' vibrations are located in the spectral region below 1700 cm^{-1}. The amide I band (mainly attributed to C=O stretching in the amide moiety) represents two components from a population of non- (or weakly) H-bonded and H-bonded moieties (observed in a pure SM monolayer at 1663 and 1642 cm^{-1}, respectively) [60]. The compression of pure SM does not influence the band positions and results only in their mutual intensity (the band at 1663 cm^{-1} weakens while the band at 1642 cm^{-1} becomes more intensive with the surface pressure increase) [60]. In the case of the 25-OH/SM ($X_{25\text{-OH}} = 0.50$) monolayer compressed to 20 mN m^{-1}, the band from the non-hydrated amide I shows a much higher intensity and is also shifted to 1649 cm^{-1}. The intensity ratio between the hydrated and non-hydrated amide I signals, observed for the mixture, is different from the spectrum of pure SM recorded at the same surface pressure and points to higher dehydration (and, as a result, condensation) of the mixed monolayer. Values of the compression moduli also support the latter conclusion. Further increases in surface pressure result in the appearance of the single wide band at 1655 cm^{-1}. This may suggest that, in 25-OH/SM mixed films, surface ordering based on H-bonding between C=O and –OH (or –NH) groups located in the interfacial region of SM molecules is disturbed. This can be explained by the fact that the C = O moiety in SM becomes preferentially involved in interactions with 25-OH molecules

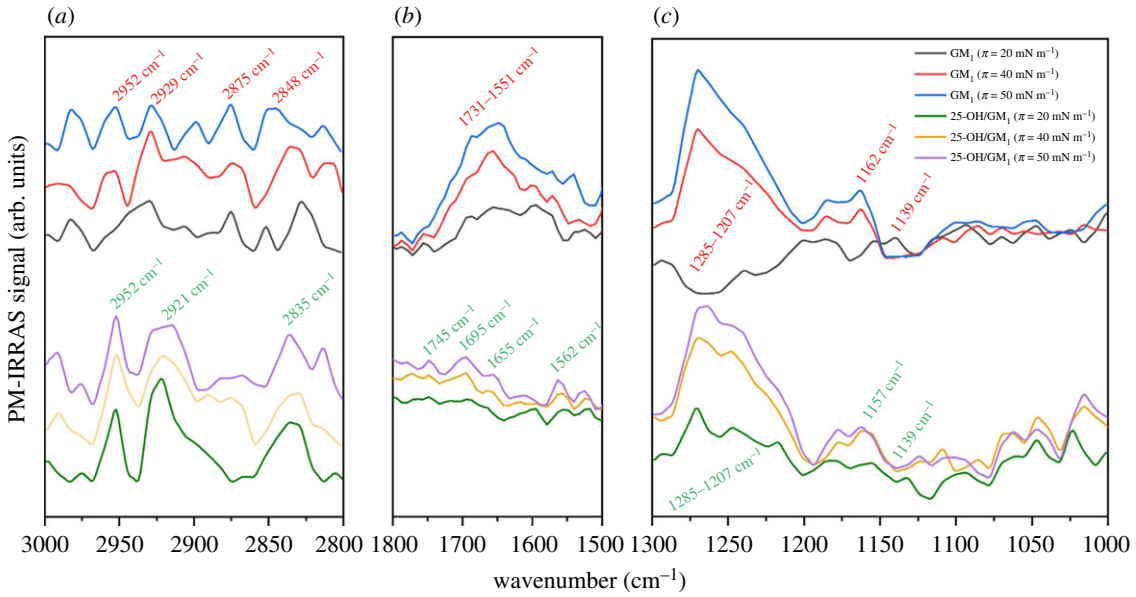

Figure 7. PM-IRRAS spectra of the 25-OH/GM_1 ($X_{25\text{-OH}} = 0.50$) monolayer compared with the spectra of pure GM_1 at selected values of the surface pressure registered in the spectral regions 3000–2800 (*a*), 1800–1500 (*b*) and 1300–1000 cm^{-1} (*c*).

rather than water or other SM molecules. A similar behaviour was observed for Chol/SM systems [61] and confirmed SM's high affinity for Chol and its derivatives. In the 1300–1000 cm^{-1} region, the signals from SM overlap with bands from vibrations of 25-OH. Namely, in the spectrum of the 25-OH/SM system, broad, positive intensive bands (1285–1223 cm^{-1}) resulting from overlapping bands from the dehydrated component of PO_2^- asymmetric stretching in SM [61], C–N stretching (amide III), C(3)–O–H scissoring in 25-OH [37] and various deformation vibrations of hydrocarbons in both molecules are visible. Interestingly, the hydrated component of the asymmetric PO_2^- band [61] is observed as a negative signal at 1217 cm^{-1} (the band is more negative at a surface pressure of 20 mN m^{-1} than at 43 mN m^{-1}). The latter suggests that SM's orientation in the mixed monolayer is different from that observed in the monolayer of the pure compound. This is additionally supported by the positive, quite strong absorption band (at 1200 cm^{-1}) from C(25)–O stretching in 25-OH.

The second analysed system is a mixture of 25-OH/GM_1 ($X_{25\text{-OH}} = 0.50$) (figure 7).

Signals in the C–H stretching region (3000–2800 cm^{-1}) in the spectra from the 25-OH/GM_1 mixture show quite well the defined bands from the CH_3 asymmetric stretching (at 2952 cm^{-1}) and CH_2 asymmetric (at *ca* 2921 cm^{-1}) and symmetric (at *ca* 2835 cm^{-1}) stretching vibrations, while the CH_3 symmetric stretching band (in contrast to the spectrum from the pure GM_1 monolayer) is almost unnoticeable. Both the shape and band position as well as their mutual intensity ratio are purely affected by the surface pressure, which suggests that compression does not influence acyl chain order in mixed monolayers. In the spectral region 1800–1500 cm^{-1}, the monolayer of pure GM_1 shows a broad absorption band resulting from C=O (amide I) and –O–C=O stretching as well as NH bending modes (amide II) [51]. As can be seen, the intensity of this signal increases with compression. The addition of 25-OH to the GM_1 monolayer causes striking changes in the analysed bands: (i) they become better defined (peaks at 1745, 1695, 1655 and 1562 cm^{-1} can be easily distinguished); however, (ii) their intensity decreases significantly. This can result from (i) a better defined surface ordering of GM_1 in the mixed monolayer and (ii) orientation changes of carbohydrate moieties in the GM_1 structure. Both effects are probably induced by the attractive interactions with 25-OH, leading to the monolayer condensation. As the GM_1 molecule possesses five carbohydrate rings in its structure, the absorption in the region 1300–1000 cm^{-1} is dominated by the bands from O–C–O asymmetric stretching, –OH deformation vibrations together with deformation vibrations of hydrocarbons as well as the amide III band (C–N stretching). Owing to the large number of infrared-absorbing functional groups in GM_1 as compared with 25-OH, it can be assumed that signals in this region mainly inform about GM_1. Regarding the pure GM_1 monolayer, it can be noted that the intensity of a broad band (1285–1207 cm^{-1}) varies significantly with surface pressure. At 20 mN m^{-1}, it is negative, while at 40 and 50 mN m^{-1} the band becomes the most intensive in the analysed region. Because of changes in the surface pressure, intensity shifts are also observed for bands at 1162 and 1139 cm^{-1}. This confirms the existence of the GM_1 molecules in the form of two different conformers that are characteristic for the liquid expanded and the liquid condensed phases [51]. In the 25-OH/GM_1 system, bands characteristic for the GM_1 conformer from the condensed liquid phase are already observed at 20 mN m^{-1}, which is also supported by the results from isotherms (lack of inflections below 47 mN m^{-1} associated with the phase transition). This also supports the hypothesis on attractive interactions with 25-OH, leading to film condensation.

3.4. Theoretical calculations

3.4.1. DFT modelling

We conducted computer simulations to quantify the energy of interaction between molecules in the 25-OH/SM and 25-OH/GM_1 systems. The first step was a quantum-chemical simulation. Using DFT modelling, we calculated the bond energy of the molecules in the dimers. This energy is defined as the difference between the dimer energy and the sum of the separated molecules. The energies

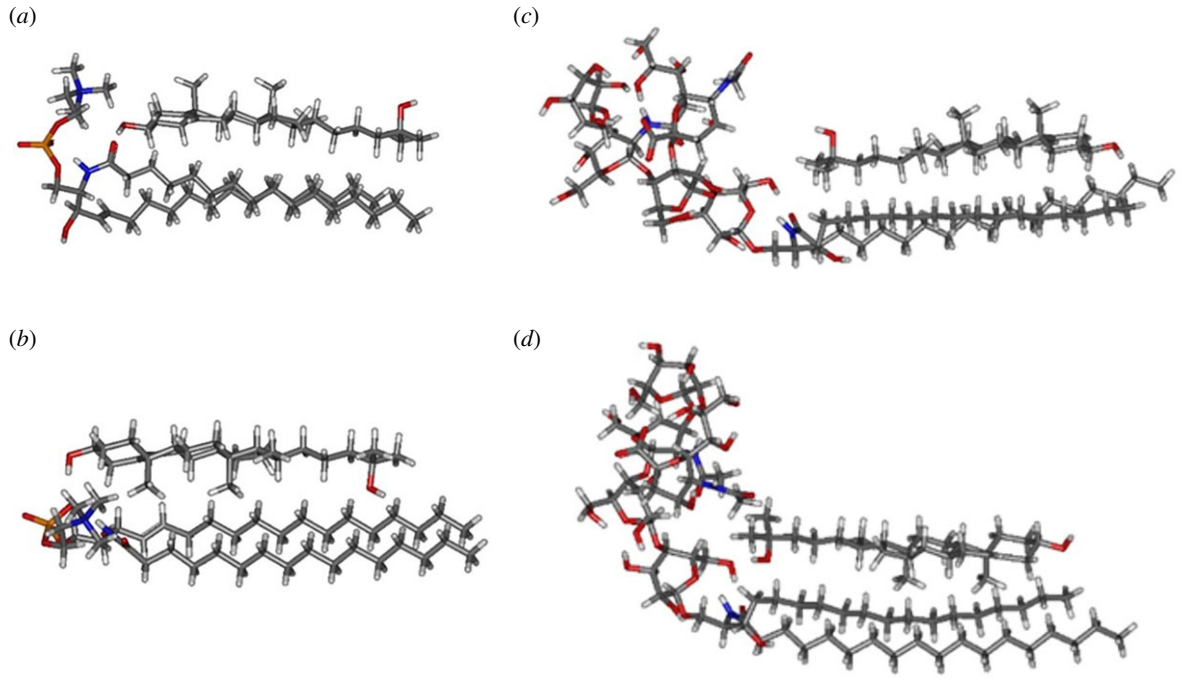

Figure 8. Models of geometrically optimized 25-OH/SM and 25-OH/GM_1 dimers calculated using the B3LYP functional with the 6–311G(d,p) basis set.

Table 1. Bond energies of 25-OH/SM and 25-OH/GM_1 dimers depending on the mutual orientation of molecules.

		binding energy (kcal mol^{-1})	
mutual orientation of molecules in the dimer		25-OH/SM	25-OH/GM_1
polar group neighbouring C(3)–OH of 25-OH	25-OH methyl groups outside	−32.67	−34.16
	25-OH methyl groups inside	−31.76	−42.11
polar group neighbouring C(25)–OH of 25-OH	25-OH methyl groups outside	−23.50	−30.18
	25-OH methyl groups inside	−22.18	−36.26

per dimer are presented in table 1. The mutual orientations of the molecules are shown in figure 8.

In the case of 25-OH/SM, the lowest bond energy is found for the arrangement with the polar group neighbouring C(3)–OH, regardless of how methyl groups in 25-OH are oriented (−32.67 kcal mol^{-1} and −31.76 kcal mol^{-1} for methyl groups oriented outwards and inwards, respectively). For the systems with the polar group neighbouring C(25)–OH, bond energies are approximately one-third lower and equal to −23.50 kcal mol^{-1} and −22.18 kcal mol^{-1} for methyl groups oriented outside and inside, respectively. In turn, for the 25-OH/GM_1 system, the most energetically preferred arrangement is with inward-facing methyl groups. The binding energies are −42.11 kcal mol^{-1} and −36.26 kcal mol^{-1} for polar groups neighbouring C(3)–OH and C(25)–OH, respectively. For outwardly directed methyl groups, the bond energies are −34.16 kcal mol^{-1} and −30.18 kcal mol^{-1} for polar groups neighbouring C(3)–OH and C(25)–OH, respectively.

3.4.2. Molecular dynamics simulations

To reproduce the experimental conditions for the investigated systems, we conducted simulations of classical molecular dynamics. The analysed monolayers consisted of 77 SM molecules and 51 25-OH molecules or 56 GM_1 molecules and 56 25-OH molecules. The average area per lipid as a function of time, showing equilibrium of the systems, is presented in electronic supplementary material, figure S6. The systems were subjected to surface tensions equal to 10, 30 or 48 mN m^{-1}. The side order of simulated monolayers is shown in figure 9. For the 25-OH/SM system with polar groups neighbouring C(3)–OH, the total potential energy is equal to −21 354 kcal mol^{-1}, while in the case of the polar group neighbouring C(25)–OH, it is equal to −21 021 kcal mol^{-1}. Such a difference is not observed in the 25-OH/GM_1 system, for which the potential energy is 35 049 kcal mol^{-1} and 35 044 kcal mol^{-1} for the polar groups neighbouring C(3)–OH and C(25)–OH, respectively.

Figure 9 shows the density profiles of the hydroxyl groups and mass centres of the polar groups of the analysed monolayers. It can be seen that for the 25-OH/SM system, when the polar group is initially adjacent to C(25)–OH, after 70 ns of simulation 30% of the oxysterols changed orientation (figure 10*b*). For the polar group's initial orientation neighbouring C(3)–OH, only 8% changed their orientation (figure 10*a*). This effect is not so significant for the 25-OH/GM_1 system. In this case, 6% and 5% of 25-OH molecules changed their initial orientation for the system with polar groups neighbouring C(25)–OH and C(3)–OH, respectively. This

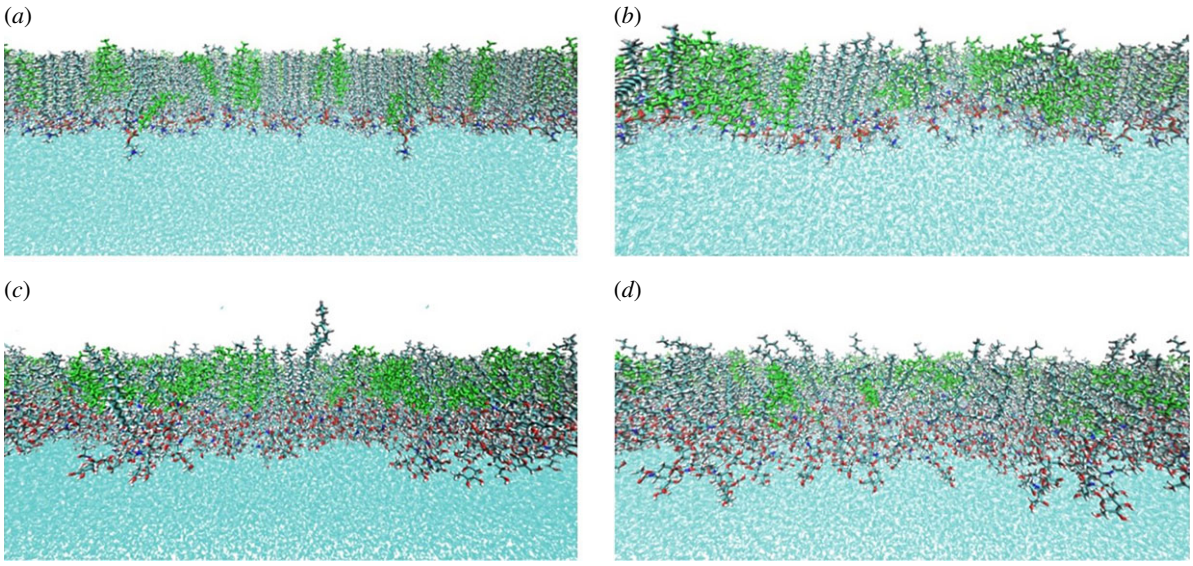

Figure 9. Monolayers obtained after 70 ns production of molecular dynamics for 25-OH/SM (*a*,*b*) and 25-OH/GM_1 (*c*,*d*) systems at 30 mN m^{-1} with different mutual orientations: polar groups neighbouring C(3)–OH (*a*,*c*) or C(25)–OH (*b*,*d*).

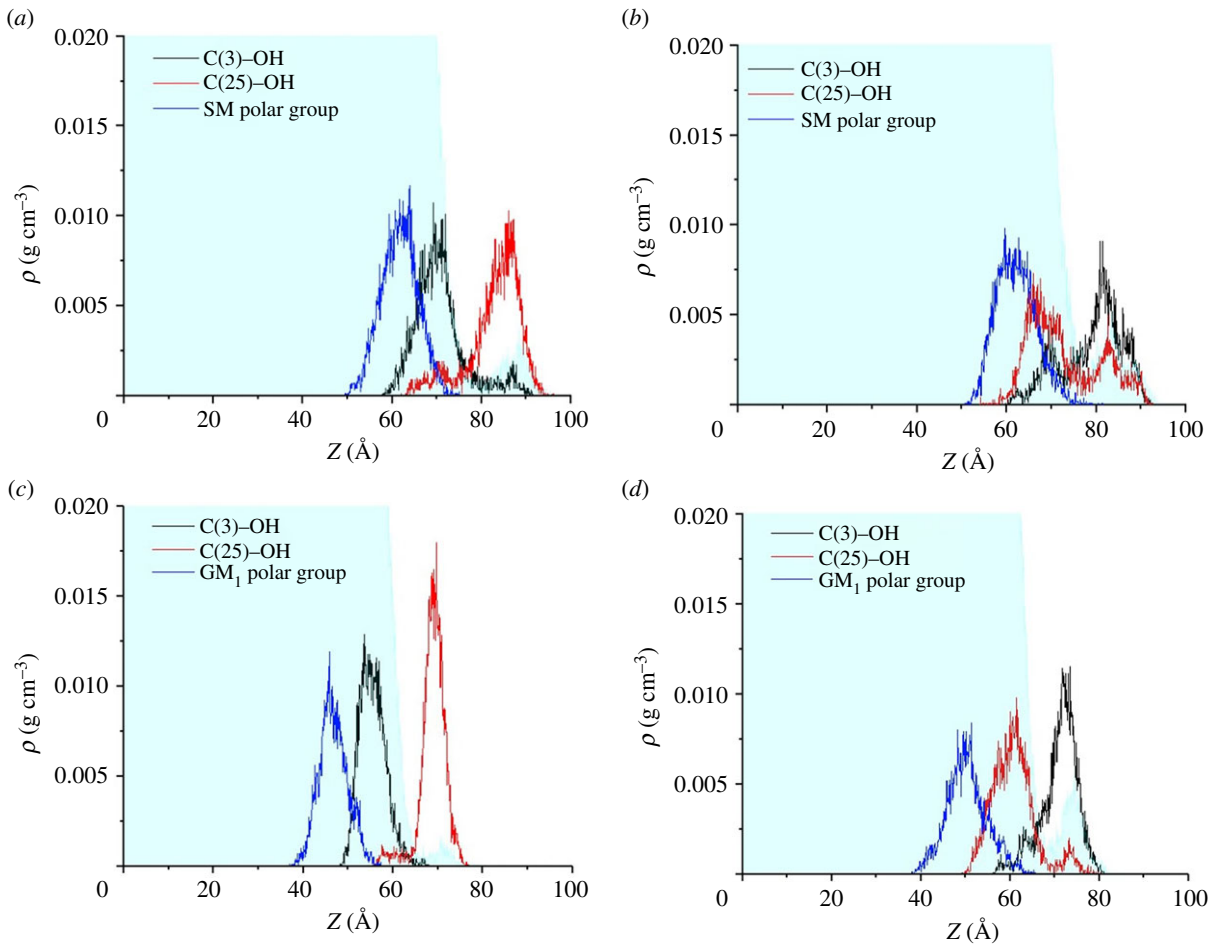

Figure 10. Density profiles of specified atoms for monolayers compressed to 30 mN m^{-1}. The left-hand side shows the 25-OH/SM (*a*) and 25-OH/GM_1 (*c*) systems with polar groups neighbouring C(3)–OH; the right-hand side presents 25-OH/SM (*b*) and 25-OH/GM_1 (*d*) systems with polar groups neighbouring C(25)–OH.

behaviour illustrates that the 25-OH/SM system with polar groups adjacent to C(3)–OH is more energetically preferred.

We also determined the order of the phospholipid chains by calculating the $|SCD|_Z$ parameter. It is defined as

$$|SCD|_Z = \frac{1/2\langle 3\cos(2\Theta)\rangle - 1}{2},$$

where Θ is the angle between the vector joining carbons C_{n-1} and C_{n+1} and the monolayer normal. Angle brackets denote a time average.

Figure 11 shows the obtained $|SCD|_Z$ values for systems with different orientations of 25-OH and surface tensions equal to 10, 30 or 48 mN m^{-1}. It can be seen that significantly higher values of the $|SCD|_Z$ parameters were obtained for

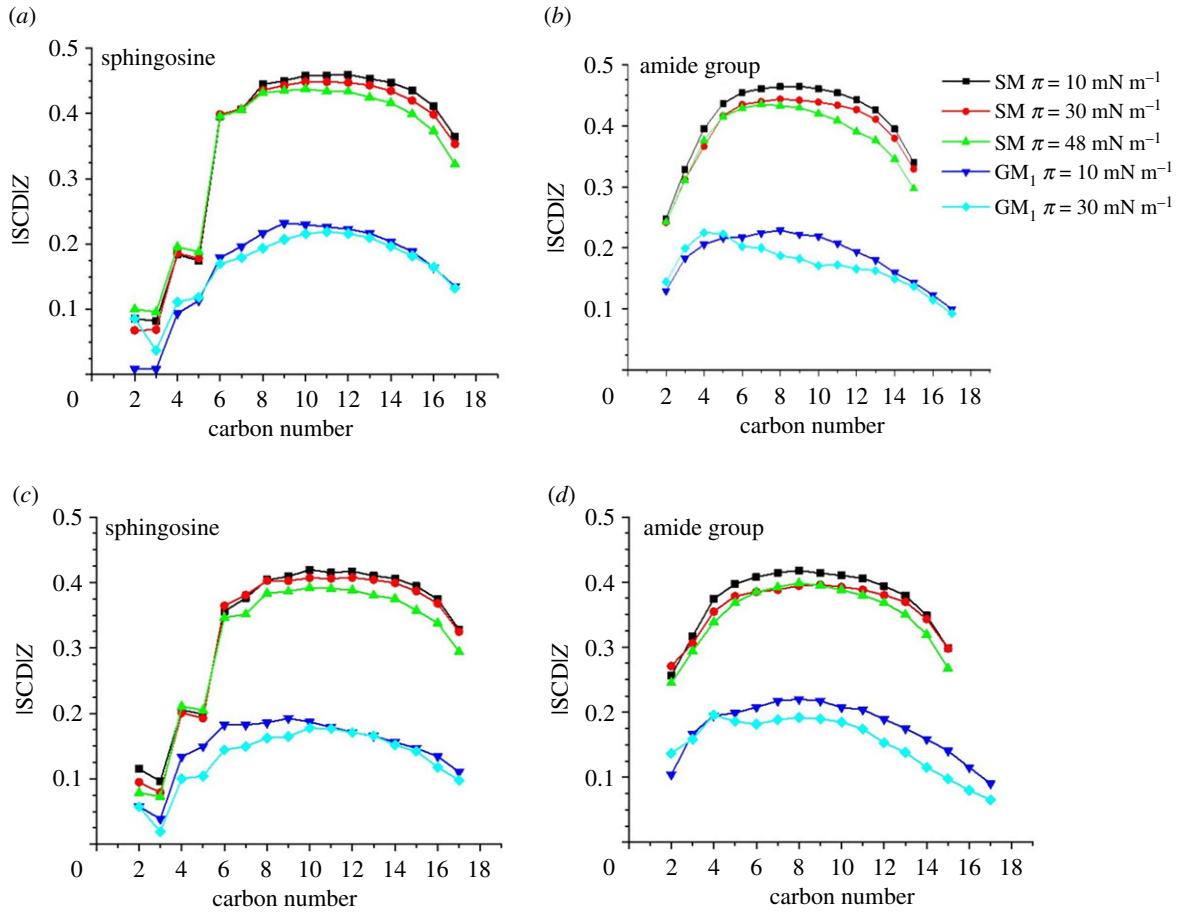

Figure 11. Values of the $|SCD|_Z$ order parameter for 25-OH/SM and 25-OH/GM_1 systems. Density profiles of specified atoms for monolayers compressed to 30 mN m^{-1}. Polar groups of SM (*a*) and GM_1 (*b*) neighbouring C(3)–OH; polar groups of SM (*c*) and GM_1 (*d*) neighbouring C(25)–OH.

25-OH/SM systems. For the 25-OH/GM_1 system and 48 mN m^{-1}, equilibrations were not obtained. It can be seen that slightly higher values were obtained for the systems with the polar group adjacent to C(3)–OH.

Systems with the lowest surface tension, i.e. 10 mN m^{-1}, are characterized by high values of the $|SCD|_Z$ parameter, which is in agreement with the experimental results. Increasing surface tension causes a slight decrease in the $|SCD|_Z$ value.

4. Summary and conclusion

In this paper, systems composed of a representative of chain-oxidized Chol, 25-OH, mixed with SM or GM_1, have been examined and compared. Several complementary methods (classical Langmuir monolayer technique based on surface pressure measurements, BAM, PM-IRRAS and theoretical calculations) gave consistent results. The most important findings are as follows.

(1) 25-OH forms surface complexes with both SM and GM_1, as indicated by thermodynamic analysis (ΔG^{exc} plots) and changes in the PM-IRRAS spectra.
(2) The introduction of 25-OH molecules into the monolayers from sphingolipids causes film stiffening (which is confirmed by the compressibility moduli, PM-IRRAS analysis and molecular dynamics).
(3) Analysis of π–*A* isotherms complemented with molecular dynamics and DFT modelling confirmed that SM enforces one specific orientation of 25-OH in surface complexes (being anchored with the C(3)–OH group to the water). PM-IRRAS results indicate that probably hydrogen bonds are formed between the interfacial region of SM and the 25-OH molecule.
(4) GM_1 allows the 25-OH to anchor to the water surface with either the C(3)–OH or C(25)–OH group and form two types of complexes. Unfortunately, in BAM images, we could not observe two collapses corresponding to the two types of complexes, probably because of the similar value of the refractive index for GM_1 and water.
(5) Compared with Chol/SM mixtures, the strength of interactions (reflected in ΔG^{exc} values) in the 25-OH/SM system is stronger (by *ca* 30%), and the monolayer is more rigid. In analogous systems with GM_1, the interactions with 25-OH are slightly weaker by 10% than in a mixture containing Chol. However, interaction strength is still of comparable order.
(6) Furthermore, in the case of ring-oxidized Chol derivatives (7α- and 7β-hydroxyChol., abbr. 7α-OH and 7β-OH) and SM interaction, their strength is weaker than in those involving 25-OH. This effect is especially pronounced for 7β-OH/SM (approx. −500 J mol^{-1}).
(7) The surface behaviour of 25-OH in mixed systems with sphingolipids may have important biological implications. A comparable strength of interactions between GM_1 and Chol versus 25-OH indicates that, if both sterols are present, they can compete for the interaction with the GM_1. In SM's case, weaker interactions with Chol than 25-OH prove that oxysterol molecules may replace Chol.
(8) The above-described changes due to incorporation of oxysterols observed in simple raft models (mimicked with the

Langmuir monolayer technique) might be generalized to the analogous processes in living natural systems.

Data accessibility. This article has no additional data.

Authors' contributions. A.W. and P.D.-L. designed the research; J.K., A.W., A.C.B. and A.F. conducted the research, A.W., J.K. and A.C.B. drafted the manuscript; A.D.P. and P.D.-L. edited the manuscript.

Competing interests. We declare we have no competing interests

Funding. This research was supported in part by PL-Grid Infrastructure. The research was financed in part by a Polish Ministry of Science and Higher Education subvention (no. 2020–N17/MNS/000019). This study was conducted using the KSV PM-IRRAS instrument funded by the European Funds for Regional Development and the National Funds of Ministry of Science and Higher Education, as part of the Operational Program Development of Eastern Poland 2007–2013, project: POPW.01.03.00–20–044/11.

References

1. Karp G, Iwasa J, Wallace M. 2016 *Karp's cell and molecular biology: concepts and experiments,* 8th edn. Hoboken, NJ: John Wiley & Sons.
2. Devaux PF, Zachowski A. 1993 Transmembrane lipid asymmetry in eukaryotes. In *New developments in lipid–protein interactions and receptor function* (eds KWA Wirtz, L Packer, JÅ Gustafsson, AE Evangelopoulos, JP Changeux), pp. 213–226. NATO ASI Series (Series A: Life Sciences), vol. 246. Berlin, Germany: Springer.
3. Lorent JH, Levental KR, Ganesan L, Rivera-Longsworth G, Sezgin E, Doktorova M, Lyman E, Levental I. 2020 Plasma membranes are asymmetric in lipid unsaturation, packing and protein shape. *Nat. Chem. Biol.* **16**, 644–652. (doi:10.1038/s41589-020-0529-6)
4. Maxfield FR, Mondal M. 2006 Sterol and lipid trafficking in mammalian cells. *Biochem. Soc. Trans.* **34**, 335–339. (doi:10.1042/BST0340335)
5. Steck TL, Lange Y. 2018 Transverse distribution of plasma membrane bilayer cholesterol: picking sides. *Traffic* **19**, 750–760. (doi:10.1111/tra.12586)
6. Oliveira RG, Calderón RO, Maggio B. 1998 Surface behavior of myelin monolayers. *Biochim. Biophys. Acta Biomembr.* **1370**, 127–137. (doi:10.1016/S0005-2736(97)00254-X)
7. Benga G, Hodarnau A, Bohm B, Borza V, Twilinca R, Dancea S, Petrescu I, Ferdinand W. 1978 Human liver mitochondria: relation of a particular lipid composition to the mobility of spin-labelled lipids. *Eur. J. Biochem.* **84**, 625–633. (doi:10.1111/j.1432-1033.1978.tb12205.x)
8. Krause MR, Regen SL. 2014 The structural role of cholesterol in cell membranes: from condensed bilayers to lipid rafts. *Acc. Chem. Res.* **47**, 3512–3521. (doi:10.1021/ar500260t)
9. Almeida PFF. 2009 Thermodynamics of lipid interactions in complex bilayers. *Biochim. Biophys. Acta Biomembr.* **1788**, 72–85. (doi:10.1016/j.bbamem.2008.08.007)
10. Sengupta P, Hammond A, Holowka D, Baird B. 2008 Structural determinants for partitioning of lipids and proteins between coexisting fluid phases in giant plasma membrane vesicles. *Biochim. Biophys. Acta Biomembr.* **1778**, 20–32. (doi:10.1016/j.bbamem.2007.08.028)
11. Jurak M. 2013 Thermodynamic aspects of cholesterol effect on properties of phospholipid onolayers: Langmuir and Langmuir–Blodgett monolayer study. *J. Phys. Chem. B* **117**, 3496–3502. (doi:10.1021/jp401182c)
12. Wydro P, Knapczyk S, Łapczyńska M. 2011 Variations in the condensing effect of cholesterol on saturated versus unsaturated phosphatidylcholines at low and high sterol concentration. *Langmuir* **27**, 5433–5444. (doi:10.1021/la105142w)
13. Jurak M, Golabek M, Holysz L, Chibowski E. 2015 Properties of Langmuir and solid supported lipid films with sphingomyelin. *Adv. Colloid Interface Sci.* **222**, 385–397. (doi:10.1016/j.cis.2014.03.008)
14. Yahi N, Aulas A, Fantini J. 2010 How cholesterol constrains glycolipid conformation for optimal recognition of Alzheimer's β amyloid peptide (Aβ1–40). *PLoS ONE* **5**, e9079. (doi:10.1371/journal.pone.0009079)
15. Lingwood D, Kaiser HJ, Levental I, Simons K. 2009 Lipid rafts as functional heterogeneity in cell membranes. *Biochem. Soc. Trans.* **37**, 955–960. (doi:10.1042/BST0370955)
16. Saha S, Anilkumar AA, Mayor S. 2016 GPI-anchored protein organization and dynamics at the cell surface. *J. Lipid Res.* **57**, 159–175. (doi:10.1194/jlr.R062885)
17. Simons K, Toomre D. 2000 Lipid rafts and signal transduction. *Nat. Rev. Mol. Cell Biol.* **1**, 31–39. (doi:10.1038/35036052)
18. Stone MB, Shelby SA, Núñez MF, Wisser K, Veatch SL. 2017 Protein sorting by lipid phase-like domains supports emergent signaling function in B lymphocyte plasma membranes. *Elife* **6**, e19891. (doi:10.7554/eLife.19891)
19. Foster LJ, Chan QWT. 2007 Lipid raft proteomics: more than just detergent-resistant membranes. *Subcell. Biochem.* **43**, 35–47. (doi:10.1007/978-1-4020-5943-8_4)
20. Campbell SM, Crowe SM, Mak J. 2001 Lipid rafts and HIV-1: from viral entry to assembly of progeny virions. *J. Clin. Virol.* **22**, 217–227. (doi:10.1016/S1386-6532(01)00193-7)
21. Choi KS, Aizaki H, Lai MMC. 2005 Murine coronavirus requires lipid rafts for virus entry and cell-cell fusion but not for virus release. *J. Virol.* **79**, 9862–9871. (doi:10.1128/jvi.79.15.9862-9871.2005)
22. Thorp EB, Gallagher TM. 2004 Requirements for CEACAMs and cholesterol during murine coronavirus cell entry. *J. Virol.* **78**, 2682–2692. (doi:10.1128/jvi.78.6.2682-2692.2004)
23. Takahashi T, Suzuki T. 2009 Role of membrane rafts in viral infection. *Open Dermatol. J.* **3**, 178–194. (doi:10.2174/1874372200903010178)
24. Li C *et al.* 2017 25-Hydroxycholesterol protects host against Zika virus infection and its associated microcephaly in a mouse model. *Immunity* **46**, 446–456. (doi:10.1016/j.immuni.2017.02.012)
25. Tricarico PM, Caracciolo I, Gratton R, D'Agaro P, Crovella S. 2019 25-Hydroxycholesterol reduces inflammation, viral load and cell death in ZIKV-infected U-87 MG glial cell line. *Inflammopharmacology* **27**, 621–625. (doi:10.1007/s10787-018-0517-6)
26. Chinnapen DJ-F, Chinnapen H, Saslowsky D, Lencer WI. 2007 Rafting with cholera toxin: endocytosis and trafficking from plasma membrane to ER. *FEMS Microbiol. Lett.* **266**, 129–137. (doi:10.1111/j.1574-6968.2006.00545.x)
27. Lingwood D, Simons K. 2010 Lipid rafts as a membrane-organizing principle. *Science* **327**, 46–50. (doi:10.1126/science.1174621)
28. Mukherjee S, Maxfield FR. 2004 Membrane domains. *Annu. Rev. Cell Dev. Biol.* **20**, 839–866. (doi:10.1146/annurev.cellbio.20.010403.095451)
29. Hac-Wydro K, Dynarowicz-Łątka P, Wydro P, Bak K. 2011 Edelfosine disturbs the sphingomyelin–cholesterol model membrane system in a cholesterol-dependent way – the Langmuir monolayer study. *Colloids Surf. B Biointerfaces* **88**, 635–640. (doi:10.1016/j.colsurfb.2011.07.055)
30. Jablin MS, Flasiński M, Dubey M, Ratnaweera DR, Broniatowski M, Dynarowicz-Łątka P, Majewski J. 2010 Effects of β-cyclodextrin on the structure of sphingomyelin/ cholesterol model membranes. *Biophys. J.* **99**, 1475–1481. (doi:10.1016/j.bpj.2010.06.028)
31. Thakur G, Pao C, Micic M, Johnson S, Leblanc RM. 2011 Surface chemistry of lipid raft and amyloid Aβ (1–40) Langmuir monolayer. *Colloids Surf. B Biointerfaces* **87**, 369–377. (doi:10.1016/j.colsurfb.2011.05.047)
32. Mesa-Herrera F, Taoro-González L, Valdés-Baizabal C, Diaz M, Marín R. 2019 Lipid and lipid raft alteration in aging and neurodegenerative diseases: a window for the development of new biomarkers. *Int. J. Mol. Sci.* **20**, 3810. (doi:10.3390/ijms20153810)
33. Michel V, Bakovic M. 2007 Lipid rafts in health and disease. *Biol. Cell* **99**, 129–140. (doi:10.1042/bc20060051)
34. Sottero B, Gamba P, Gargiulo S, Leonarduzzi G, Poli G. 2009 Cholesterol oxidation products and disease: an emerging topic of interest in medicinal chemistry. *Curr. Med. Chem.* **16**, 685–705. (doi:10.2174/092986709787458353)

35. Wnętrzak A, Makyła-Juzak K, Filiczkowska A, Kulig W, Dynarowicz-Łątka P. 2017 Oxysterols versus cholesterol in model neuronal membrane. I. The case of 7-ketocholesterol. The Langmuir Monolayer Study. *J. Membr. Biol.* **250**, 553–564. (doi:10.1007/s00232-017-9984-8)
36. Chachaj-Brekiesz A, Wnętrzak A, Lipiec E, Dynarowicz-Łątka P. 2019 Surface interactions determined by stereostructure on the example of 7-hydroxycholesterol epimers – the Langmuir monolayer study. *Biochim. Biophys. Acta Biomembr.* **1861**, 1275–1283. (doi:10.1016/j.bbamem.2019.05.005)
37. Wnętrzak A, Chachaj-Brekiesz A, Kobierski J, Karwowska K, Petelska AD, Dynarowicz-Łątka P. 2020 Unusual behavior of the bipolar molecule 25-hydroxycholesterol at the air/water interface – Langmuir monolayer approach complemented with theoretical calculations. *J. Phys. Chem. B* **124**, 1104–1114. (doi:10.1021/acs.jpcb.9b10938)
38. Frisch MJ *et al.* 2016 *Gaussian 16, Revision B.01*. Wallingford, CT: Gaussian Inc.
39. Becke AD. 1993 Density-functional thermochemistry. III. The role of exact exchange. *J. Chem. Phys.* **98**, 5648–5652. (doi:10.1063/1.464913)
40. Lee C, Yang W, Parr RG. 1988 Development of the Colle-Salvetti correlation-energy formula into a functional of the electron density. *Phys. Rev. B* **37**, 785–789. (doi:10.1103/PhysRevB.37.785)
41. Vosko SH, Wilk L, Nusair M. 1980 Accurate spin-dependent electron liquid correlation energies for local spin density calculations: a critical analysis. *Can. J. Phys.* **58**, 1200–1211. (doi:10.1139/p80-159)
42. Stephens PJ, Devlin FJ, Chabalowski CF, Frisch MJ. 1994 Ab initio calculation of vibrational absorption and circular dichroism spectra using density functional force fields. *J. Phys. Chem.* **98**, 11 623–11 627. (doi:10.1021/j100096a001)
43. McLean AD, Chandler GS. 1980 Contracted Gaussian basis sets for molecular calculations. I. Second row atoms, Z = 11–18. *J. Chem. Phys.* **72**, 5639–5648. (doi:10.1063/1.438980)
44. Krishnan R, Binkley JS, Seeger R, Pople JA. 1980 Self-consistent molecular orbital methods. XX. A basis set for correlated wave functions. *J. Chem. Phys.* **72**, 650–654. (doi:10.1063/1.438955)
45. Grimme S, Antony J, Ehrlich S, Krieg H. 2010 A consistent and accurate ab initio parametrization of density functional dispersion correction (DFT-D) for the 94 elements H-Pu. *J. Chem. Phys.* **132**, 154104. (doi:10.1063/1.3382344)
46. Case DA *et al*. 2018 *Amber18*. San Francisco, CA: University of California.
47. Wang J, Wolf RM, Caldwell JW, Kollman PA, Case DA. 2004 Development and testing of a general amber force field. *J. Comput. Chem.* **25**, 1157–1174. (doi:10.1002/jcc.20035)
48. Jorgensen WL, Chandrasekhar J, Madura JD, Impey RW, Klein ML. 1983 Comparison of simple potential functions for simulating liquid water. *J. Chem. Phys.* **79**, 926–935. (doi:10.1063/1.445869)
49. Dynarowicz-Łątka P, Kita K. 1999 Molecular interaction in mixed monolayers at the air/water interface. *Adv. Colloid Interface Sci.* **79**, 1–17. (doi:10.1016/S0001-8686(98)00064-5)
50. Pagano R, Gershfeld N. 1972 A millidyne film balance for measuring intermolecular energies in lipid films. *J. Colloid Interface Sci.* **41**, 311–317. (doi:10.1016/0021-9797(72)90116-6)
51. Röefzaad M, Klüner T, Brand I. 2009 Orientation of the GM1 ganglioside in Langmuir-Blodgett monolayers: a PM IRRAS and computational study. *Phys. Chem. Chem. Phys.* **11**, 10 140–10 151. (doi:10.1039/b910479h)
52. Wnętrzak A, Makyła-Juzak K, Chachaj-Brekiesz A, Lipiec E, Romeu NV, Dynarowicz-Łątka P. 2018 Cyclosporin A distribution in cholesterol-sphingomyelin artificial membranes modeled as Langmuir monolayers. *Colloids Surf. B Biointerfaces* **166**, 286–294. (doi:10.1016/j.colsurfb.2018.03.031)
53. Marsh D. 2007 Lateral pressure profile, spontaneous curvature frustration, and the incorporation and conformation of proteins in membranes. *Biophys. J.* **93**, 3884–3899. (doi:10.1529/BIOPHYSJ.107.107938)
54. Schmidt TF, Caseli L, Oliveira ON, Itri R. 2015 Binding of methylene blue onto Langmuir monolayers representing cell membranes may explain its efficiency as photosensitizer in photodynamic therapy. *Langmuir* **31**, 4205–4212. (doi:10.1021/acs.langmuir.5b00166)
55. Stunges GM, Martin CS, Ruiz GCM, Oliveira ON, Constantino CJL, Alessio P. 2017 Interaction between 17 α-ethynylestradiol hormone with Langmuir monolayers: the role of charged headgroups. *Colloids Surf. B Biointerfaces* **158**, 627–633. (doi:10.1016/j.colsurfb.2017.07.034)
56. MacPhail RA, Strauss HL, Snyder RG, Eiliger CA. 1984 C-H stretching modes and the structure of n-alkyl chains. 2. Long, all-trans chains. *J. Phys. Chem.* **88**, 334–341. (doi:10.1021/j150647a002)
57. Mendelsohn R, Brauner JW, Gericke A. 1995 External infrared reflection absorption spectrometry of monolayer films at the air-water interface. *Annu. Rev. Phys. Chem.* **46**, 305–334. (doi:10.1146/annurev.pc.46.100195.001513)
58. Payan S, Desbat B, Destrade C, Nguyen HT. 1996 Study of Langmuir and Langmuir-Blodgett films of ferroelectric liquid crystals by Fourier transform infrared and polarization modulated infrared reflection absorption spectroscopies. *Langmuir* **12**, 6627–6631. (doi:10.1021/la960195h)
59. Leverette CL, Dluhy RA. 2004 Vibrational characterization of a planar-supported model bilayer system utilizing surface-enhanced Raman scattering (SERS) and infrared reflection-absorption spectroscopy (IRRAS). *Colloids Surf. A Physicochem. Eng. Asp.* **243**, 157–167. (doi:10.1016/j.colsurfa.2004.05.020)
60. Vázquez RF, Daza Millone MA, Pavinatto FJ, Fanani ML, Oliveira ON, Vela ME, Maté SM. 2019 Impact of sphingomyelin acyl chain (16:0 vs 24:1) on the interfacial properties of Langmuir monolayers: a PM-IRRAS study. *Colloids Surf. B Biointerfaces* **173**, 549–556. (doi:10.1016/j.colsurfb.2018.10.018)
61. Villalaín J, Ortiz A, Gómez-Fernández JC. 1988 Molecular interactions between sphingomyelin and phosphatidylcholine in phospholipid vesicles. *Biochim Biophys Acta* **941**, 55–62. (doi:10.1016/0005-2736(88)90213-1)